Review of Computer Engineering Research
2023 Vol. 10, No. 3, pp. 96-109
ISSN(e): 2410-9142
ISSN(p): 2412-4281
DOI: 10.18488/76.v10i3.3495

Image-based MRI detection of brain tumours using convolutional neural networks

G. Preethi[1]
Thangamma NG[2+]
S. Perumal Sankar[3]
Md. Abul Ala Walid[4]
D. Suganthi[5]
K. Deepthika[6]

[1]*Department of Computer Science and Applications, Periyar Maniammai Institute of Science and Technology, India.*
Email: preethig@pmu.edu
[2]*Computer Science, St.Joseph's College (Arts & Science), India.*
Email: Ngthangam@gmail.com
[3]*Department of Electronics, Toc H Institute of Science of Science and Technology, India.*
Email: spsankar2004@gmail.com
[4]*AI Developer, Foursteps Training Solutions Chennai, Tamilnadu, India.*
Email: abulalawalid@gmail.com
[5]*Department of Computer Science, Saveetha College of Liberal Arts and Sciences, SIMATS, Thandalam, Chennai, India.*
Email: suganthiphd@gmail.com
[6]*Department of CSE, Dr.N.G.P Institute of Technology, Coimbatore, India.*
Email: deepthi.karuppusamy@gmail.com

(+ Corresponding author)

Article History
Received: 20 June 2023
Revised: 18 September 2023
Accepted: 25 September 2023
Published: 6 October 2023

Keywords
BRATS
Convolutional neural network
MRI image
Tumor
Wavelet transform.

ABSTRACT

Rapid and uncontrolled cellular proliferation is what distinguishes a brain tumor. Unfortunately, brain tumors cannot be prevented other than via surgery. As predicted, deep learning may help diagnose and cure brain cancers. The segmentation approach has been widely studied for brain tumor removal. This uses the segmentation approach, one of the most advanced methods for object detection and categorization. To efficiently assess the tumor's size, an accurate and automated brain tumor segmentation approach is needed. We present a fully automated brain tumor separation method for imaging investigations. The approach has been developed with convolutional neural networks. The Multimodal Brain Tumor Image Segmentation (BRATS) datasets tested our strategy. This result suggests that DL should investigate heterogeneous MRI image segmentation to improve brain tumor segmentation accuracy and efficacy. This study may lead to more accurate medical diagnoses and treatments. Researchers in this study also found a way to automatically find cancerous tumours by using the Grey Level Co-Occurrence Matrix (GLCM) and discrete wavelet transform (DWT) to find features in MRI images. They then used a CNN to guess the final prognosis. The preceding section details this technique. When compared to the other algorithm, the CNN method uses computer resources better.

Contribution/Originality: The results of this study suggest that DL should look into heterogeneous MRI image segmentation to fix the problems with brain tumor segmentation not working well or accurately enough. In the current investigation, the neural network is trained using the MRI image dataset, and then segmentation losses are detected using soft dice loss. The model is then trained to correct these losses and return a segmented version of the input image. The initial step in the segmentation process involves slicing the 3D MRI model into smaller 3D sub-models.

1. INTRODUCTION

The uncontrolled and abnormal multiplication of bodily cells is one of the defining characteristics of cancer. A brain tumor is a collection of abnormal brain tissue that results from unchecked cell development and division. Although they are not particularly frequent, brain tumors are almost always fatal.

The ultimate purpose of analyzing brain tumor images is to extract crucial clinical data and diagnostic features unique to each individual patient. Once the disease has indeed been detected and localized, the information contained in the multi-dimensional image data can be used to guide and monitor interventions, providing invaluable insight into diagnosis of diseases, staging, and therapeutic interventions [1]. To visually depict these steps, a pyramid shape works well. Different methods of data processing, extraction, labelling, and representation are needed at each tier of the pyramid. As an additional step towards obtaining useful medical experience or datasets for diagnosing diseases and making decisions, a good standard of abstraction in the representation of the information is required. High-performance computing infrastructure, including fast processing units, collection, connection, image digital display, and software, is required for effective management, processing, visualization, and assessment of the obtained datasets. It is crucial to segment relevant anatomical regions for diagnosis in MRI images. The segmentation of anatomical regions and structures is of primary interest here. Although we understand that the MRI image of human tissue has a homogeneous intensity and that the structure of each tissue is interconnected, we also understand that the small intensity adjustments and straightened boundaries between both tissues make it difficult to distinguish between adjacent tissues. Due to the non-uniform essence of MRI, density segmentation utilising global thresholding fails to accurately segment MRI images.

Automatically segmenting brain tumours is difficult due to two factors: (1) Gliomas are distinguishable from other tumours because of their growing rate, lack of contrast, and antenna-like form. Additionally, their ill-defined borders make it tough to isolate gliomas from the normal tissue around them. (2) Brain tumours can develop in virtually any area of the brain and can be of varying sizes. Numerous investigators have suggested solutions to address the issues posed by the systemic heterogeneity of brain tumours [2], as mentioned above. To reliably identify and section brain lesions using Fluid Attenuated Inversion Recovery (FLAIR) MRI data, Zeineldin, et al. [3] implemented an innovative deep learning approach called DeepSeg. Given the complexity of the problem, the study of how best to implement automated segmentation technology has attracted the interest of many academics and grown into a significant area of study. Therefore, large-scale segmentation can proceed more quickly with the help of automatic brain tumour segmentation. With the above diversity in brain tumour architecture in mind, it is imperative that a mechanism for the automatic segmentation of brain tumours be proposed.

Sangeethaa [4] uses a learning technique to represent meaningful features gleaned from data collected using a variety of modalities as part of the knowledge transfer process. A generative adversarial network (GAN) learning scheme was used to look for patterns in the data from each modality. This helped with the transfer of knowledge. The problem of skewed data in medical brain volume was addressed by Zhou, et al. [5], who developed the One-pass Multi-Task Network (OM-Net). Learned discriminative and joint characteristics depend on OM-shared Net's and task-specific parameters. The OM-Net optimization procedure makes use of both teaching and online learning data transfer strategies. Additionally, the results of predictions are shared between tasks using a cross-task guided attention (CGA) module.

Convolutional neural networks have been developed to address many difficult tasks as machine learning and pattern matching have progressed. There have been significant advancements in areas such as classification and target identification. Medical image processing is also an exciting frontier for deep learning technology. Numerous academic and commercial studies on the segmentation of medical images have been created so far. Although VNet Milletari, et al. [6] perform well at segmenting single-modal images, it still has some problems when it comes to segmenting multi-modal images.

To segment brain tumour images, for example, deep convolutional neural networks (DCNN) have demonstrated satisfactory performance in recent years [7-10]. However, it can be difficult to gather a significant quantity of training images with professional captions; this is a need for several DCNN techniques. This requirement can make it particularly difficult to acquire data from multiple organizations at once. In order to give researchers a chance to evaluate and compare various background subtraction algorithms for brain tumors, we've compiled this dataset.

The rest of this piece of writing is organized as follows: We address the relevant projects in Chapter 2. In Section 3, a suggested architecture for a convolutional neural network is provided for the readers' consideration. The results are evaluated in great detail and are given below. Section 5 presents a comprehensive overview of the study's findings and recommendations.

2. RELATED WORK

Particularly challenging for DCNN algorithms is the requirement for a great number of training instances for specialist annotations. This is especially true when attempting to combine data from a variety of different sources. Utilizing non-linear and non-MRI scans for the separation of inherently diversified brain cancer sub-regions [11, 12], the Multi-modal Brain Tumor Segmentation Challenge (BraTS) was arranged in order to provide a variety of information to the scientific formation and a structure to start comparing and comparing different based segmentation methodologies for tumours. This was done as part of the Multi - modal Brain Tumor Segmentation Challenge (BraTS). For the 2018 competition, participants were given access to 191 test cases, 285 training instances, and 66 validation cases. It should not be surprising that DCNN-based models have established themselves as the gold in BraTS competitions [2, 13]. The review by Balafar, et al. [13] discusses magnetic resonance imaging, imaging modalities, and techniques for segmentation, inhomogeneity correction, and noise reduction. We wrap off by talking about the direction of upcoming research in brain segmentation.

3D U-Net Çiçek, et al. [14], a three-dimensional variant of U-Net Ronneberger and Fischer [15], which uses sophisticated convolutional neural networks to segment three-dimensional data and makes great segmentation results through the use of an encoder-decoder architecture, was the first method to be proposed. In the end, V-Net [6, 16] was the first to propose the error function known as Dice Loss, and the team building was adjusted in line with Dice coefficients to arrive at a level that is able to handle the presence of a considerable imbalance between the background and foreground voxels.

According to a recently published article [17], making improvements to the various instructional and evaluation details that are based on the original U-Net can produce results that are resilient and intended to sustain pressure. Despite the fact that many new methods, such as the densely networked connect (Dense-Net), have been suggested that perform better than the U-Net at object segmentation, this is still the case [18, 19]. For example, the densely connected network. The work in Ranjbarzadeh, et al. [20] offers a thorough analysis of current Artificial Intelligence (AI) techniques for MRI image-based brain tumor diagnosis. There are three categories of AI methods: Deep Learning (DL), Supervised, and Unsupervised.

Ranjbarzadeh, et al. [20] built a multi-level neural CNN to acquire visual multi-level data in order to accomplish image segmentation. This was accomplished by adding an auxiliary classifier to the Multi-Level Deep Medical (MLDM) and U-Net networks. The results obtained by DSC, Positive Predictive Value (PPV), and True Positive Rate (TPR) were all very similar: 83%, 73%, and 85%. Zhou, et al. [21] and Zhou and Siddiquee [22] presented a variety of nested, closely packed connection approaches as a means of linking the encoder as well as the decoder networks in an effort to close the semantic gap that exists between the feature mapping of the two sets of networks. Chen, et al. [23] came up with two different iterations of recursive neural networks that were based on the U-Net. The results of the experiments demonstrate that the efficiency of U-Net is significantly improved when coupled with one of the two different methods of network segmentation. This is in contrast to the effectiveness of U-Net when used on its own.

Xu, et al. [24] were able to greatly broaden the scope of the accessible context by merging the U-Net with Long- and short-term components. This allowed them to significantly improve accuracy. The up-sampling layer and the down-sampling layer are both essential components of FCN [22, 25]. The map of the U-feature Net is derived from the architecture of the network by down sampling its layers [26, 27].

A three-dimensional CNN architecture was proposed by Urban, et al. [28] as a means of achieving multi-modal MRI glioma segmentation. A CNN Zhou, et al. [5] are given multimodality 3D patches that have been generated from the various types of brain MRI in order to make a prediction about the tissue label of the centre voxel of the cube. The input contains information on the spatial intensity in three dimensions, in addition to an additional dimension for MRI modalities [29].

The study by Kurian and Juliet [30] suggests a unique method for quickly and accurately identifying brain cancers termed Lee sigma filtered histogram segmentation (LSFHS). Preprocessing, segmentation, feature extraction, and classification are the foundations of the LSFHS approach.

The proposed network uses unpaired adversarial training [31] to tackle the problem of labelling massive datasets. The total tumour, the tumor's core, and its growth into surrounding tissue all have dice values of 0.94, while the core's value is 0.85 and the growing portion's value is 0.93. Total tumour sensitivity is 0.91, core tumour sensitivity is 0.86, and enhancing tumour sensitivity is 0.95, as reported by a recent study [30].

Using results from BraTS 2018 and ISLES 2018, the proposed model was shown to generate useful results [32].

3. PROPOSED METHODOLOGY

3.1. Dataset Collection

The BraTS2019, BraTS2020, and BraTS2021 multimodal brain tumour datasets were extensively used in the experiments. Using 3D MRI datasets annotated by medical professionals as Ground Truth, the BraTS challenge seeks to evaluate state-of-the-art methods for conceptual brain tumour segmentation. The challenge supplies all three data sets. BraTS 2019 contains 335 brain image samples, each of which is derived from four separate MRI scans. T1, T1-ce, T2, and T2 liquid inversion recovery (FLAIR) are all types of magnetic resonance imaging (MRI) scans (Flair). All of the modes share the same 155 inches of volume, which is fairly evenly distributed across a 240 by 240 grid. Background, necrotic and non-enhancing cancers, peritumoral edoema and GB-enhancing cancers are the four types of labels used for segmenting tumour region. There are 1251 training cases and 219 validation cases in the BraTS 2021 dataset, while there are 369 training cases and 125 verification cases (both of which are unlabeled) in the BraTS 2020 dataset. These two figures are related to the process of verifying an individual's identity on the internet (unlabeled, for online validation). Each year's report from BraTS 2020, 2021, and 2019 contains the same basic data, with the exception of the total number of incidents recorded. Pictures like the one shown in Figure 1 can be found throughout the BraTS archive.

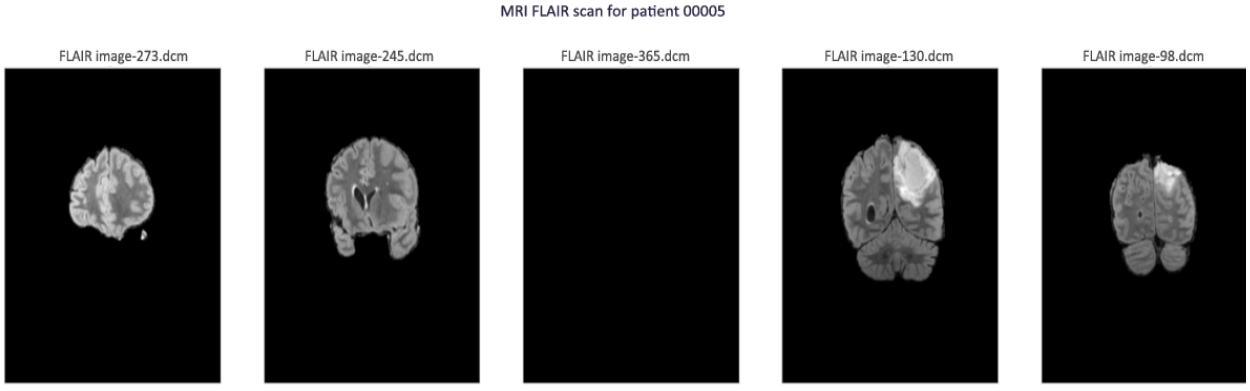

Figure 1. MRI FLAIR scan.

3.2. Data Pre-Processing and Augmentation

The role of the individual being digitised, the scanning process, and many other unknown factors can all contribute to fluctuations in the MR image's brightness. What this means is that a range of intensities may coexist within a single tissue. A common term for this is "offset field." The MR image will be completely ruined by such a low-frequency, smoothed, poor signal. There is some inconsistency in the magnetic field generated by the MRI machine due to the presence of the bias field. Every photo-processing algorithm will return inaccurate results if the alleviate field is not modified. Pre-processing is required prior to segmentation or classification in order to remove the impact of the offset field.

Figure 2 illustrates the pre-processing steps for the MR image.

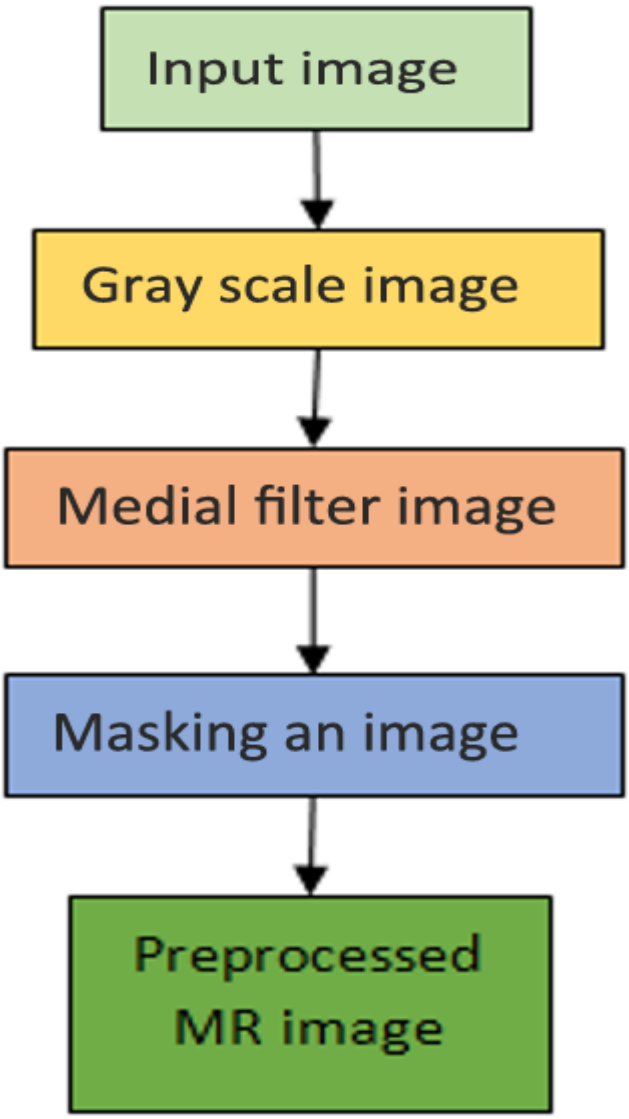

Figure 2. Preprocessing steps for the MR image.

In order to increase contrast, clean up data, and improve image quality, MR images undergo pre-processing. Using the median filter helps to eliminate irrelevant information while also reducing noise. To effectively remove noise from Magnetic Resonance (MR) images while keeping fine details intact, a non-linear filtering method known as median filtering is recommended. Image preprocessing steps for an MR scan are shown in Figure 3.

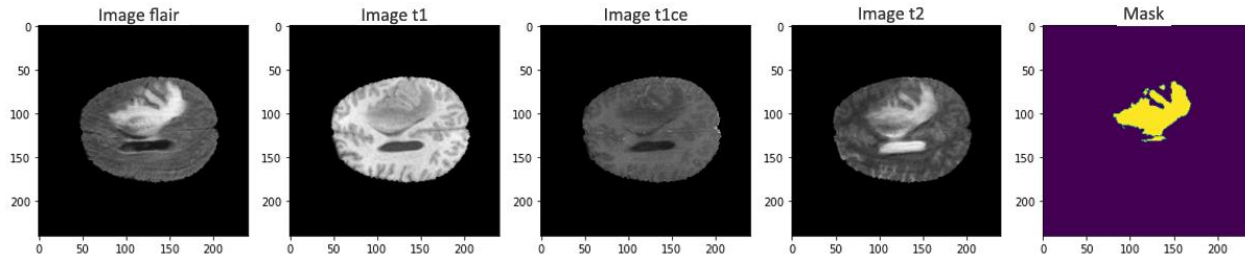

Figure 3. Preprocessing steps of MRI image.

In order to improve the quality of an MR image, the image must be preprocessed by I converting it to a lighter than concrete grayscale, and (ii) applying a median filter to remove noise using Equation 1.

$$f(i,j) = median_{(s,t)\in Sxy}\{g(r,s)\} \quad (1)$$

The sharp edges of an MR image are brought out by applying a high pass filter to it. The high-pass filter's mask can be calculated with Equation 2. To create the final enhanced MR image, we simply overlay the one with the identified edges on top of the original.

$$\begin{bmatrix} -1 & 2 & -1 \\ 0 & 0 & 0 \\ 1 & -2 & 1 \end{bmatrix} \quad (2)$$

3.3. Convolutional Neural Network

Deep learning (DL) models have the ability to learn sophisticated depictions of input images thanks to their hierarchical structure. To explain, convolutional neural networks (CNNs) have been shown to be the most efficient DL method for analyzing medical images, and widely-used explanatory sets of data are readily available. A similar annotated dataset is lacking, however, in the medical field of imaging.

3.4. Layer of Convolution

The primary processing stage is the convolutional layer, and it is responsible for figuring out what distinguishes one word from another. In this step, the feature map is generated by adding a filter to the input neuron that is specific to the data and the task at hand. It employs a neuron's activation function to introduce nonlinearity. It has the ability to decode visual data and is sensitive to very small input regions. Key components of the convolutional layer include the number of neurons, stride, dilation, and padding. Where n is the total number of filters, F is the temporal size of the filter, P is the extra space, and S is the step forwards, we have a formula for describing the size of the output image given an input image of size.

$$g(out) = \frac{g-E+2Q}{T} + 1 \quad (3)$$

$$u(out) = \frac{u-E+2Q}{T} + 1 \quad (4)$$

$$f(out) = n \quad (5)$$

3.5. Batch Normalization (BN) Layer

It allows the architecture's layers to learn more autonomously. This layer's primary responsibility is to normalize the results of the previous layer. Because of its usefulness in regularization, it's possible to employ it to circumvent the over fitting problem. The layer's responsibility is to maintain uniformity between the sequence model's inputs and outputs. This layer can be included in the model after the sequential model has been created, between the previous and next layers, or after the pooling and convolution layers. Consider the following in order to make the mathematics underpinning individual layers of BN more straightforward: In the beginning of each training phase, the input is initially normalized by reducing the mean and splitting it by the mean difference. These two values are both based on

the data from the most recent mini batch. After that, a scaling offset and a scaling coefficient are applied to the data. Because of this, we are capable of adding the given formula to the batch regularization process:

$$x = \alpha \odot x - \mu + y \quad (6)$$

The learning parameters α and μ are computed as follows:

$$\mu = 1 \sum_{x \in \beta} x \quad (7)$$

$$\alpha = 1 \sum_{x \in \beta} (x - \mu)^2 + C \quad (8)$$

Where the estimates of the variance are multiplied by a constant greater than zero in order to avoid division by zero.

There are a total of six layers in a convolutional neural network (CNN) model, including four convolution layers, one fully connected layer, and one output layer. There are also six Batch Normalization layers, six ReLU activation layers, three dropout layers, a flattening layer, and a max-pooling layer. The model is taught in a series of hidden layers how to instantly obtain such hierarchy features. When applied to the outputs of the suggested model's output layer, a softmax function generates a four-dimensional vector that corresponds to four distinct types of brain tumours, which can then be classified. To preserve the detection performance of existing pretrained networks, a primary goal of developing such a highly specialised system is to reduce the learning rate and the number of variables.

All convolution layers share the same padding, so if you feed in a 224 224 x 3 image, for example, the first convolution will convolve it with 64 3 x 3 kernels to produce a 224 x 224 x 64 volume. Next, the throughput of the initial convolutional layer undergoes batch normalisation, followed by ReLU activation. To achieve 222 x 222 64 volume, max pooling, the same Batch Normalization (BN) layer, and a dropout layer with a loss of 0.35, the output of the previous layer is fed into a convolutional layer and convolved with 64 kernels of size 3 x 3, then activated in the same way. To use a max-pooling layer with a filter size of 2 x 2 and a stride of 2, a lower-dimensional output volume of size 111 x 111 x 64 is generated. The output volume is 54 x 54 64, and it is reached by repeating the first process twice, then the second, and finally the first again. Finally, activation and batch normalization are carried out after a dropout of 0.3. The final layer's output is directly connected to four neural connections, with the accuracy and completeness of the final class label being the deciding factors. In Table 1, we summaries the proposed model's layer descriptions and tunable parameters. Graphs of training precision and loss are presented in Figures 4 and 5, respectively.

A typical neural network would struggle to scale the image properly. Convolution in a neural network, on the other hand, can be used to resize images. Input layers, convolution layers, and rectified linear units are the components that make up convolutional neural networks, sometimes known as CNNs (ReLu). An image is first segmented into a number of convolution sheet areas before being used as input. In the event that it is required, a pooling layer can take the place of the ReLu layer, which is in charge of activating the component features. As one can infer from the name of the layer, the primary purpose of the max pooling is to collect samples. In the final layer, scores or points are shown as a randomized number between 0 and 1, with 0 being the highest possible score. Input layers, convolution layers, and rectified linear units are the components that make up convolutional neural networks, sometimes known as CNNs (ReLu). An image is first segmented into a number of convolution sheet areas before being used as input. In the event that it is required, a pooling layer can take the place of the ReLu layer, which is in charge of activating the component features. As one can infer from the name of the layer, the primary purpose of the max pooling is to collect samples. In the final layer, scores or points are shown as a randomized number between 0 and 1, with 0 being the highest possible score.

The classification of brain tumours is depicted in a network diagram (Figure 3). To organise the vast collection of pictures, we use labels (tumour, normal-appearing images, etc.). Pre-processing, feature extraction, and classification are performed during training, after which a prediction model is created. Images are resized and labelled for the training phase in the pre-processing phase. As a final step, a neural convolution network is used for cancers of the brain to be detected automatically.

Every part of the model, down to the final layer, has been trained with the untrained data set. This is not only a waste of time but could also lower the quality of the end results. This issue is circumvented by employing a model-pertained brain dataset. When putting the conceptual method into practice, only the very last layer is trained. Because of this, the proposed framework is faster and more efficient in its calculations.

For calculating a loss function, the algorithm with the steepest descent is used. Classification results can be obtained by adding a scoring feature to the original, unprocessed pixel image. The loss function is applied to a certain collection of parameters in order to arrive at a quality estimate. It is essential that the regression coefficients used in the training data be accepted as valid. Improving precision relies heavily on attempts to compute the loss function. Accuracy decreases as the loss function grows in size. Similar to how accuracy increases when the error function decreases, this holds true whenever the error function is small. A descending gradient algorithm is used to estimate the loss function's value, and then the steepest descent value is used repeatedly to compute the loss function's gradient.

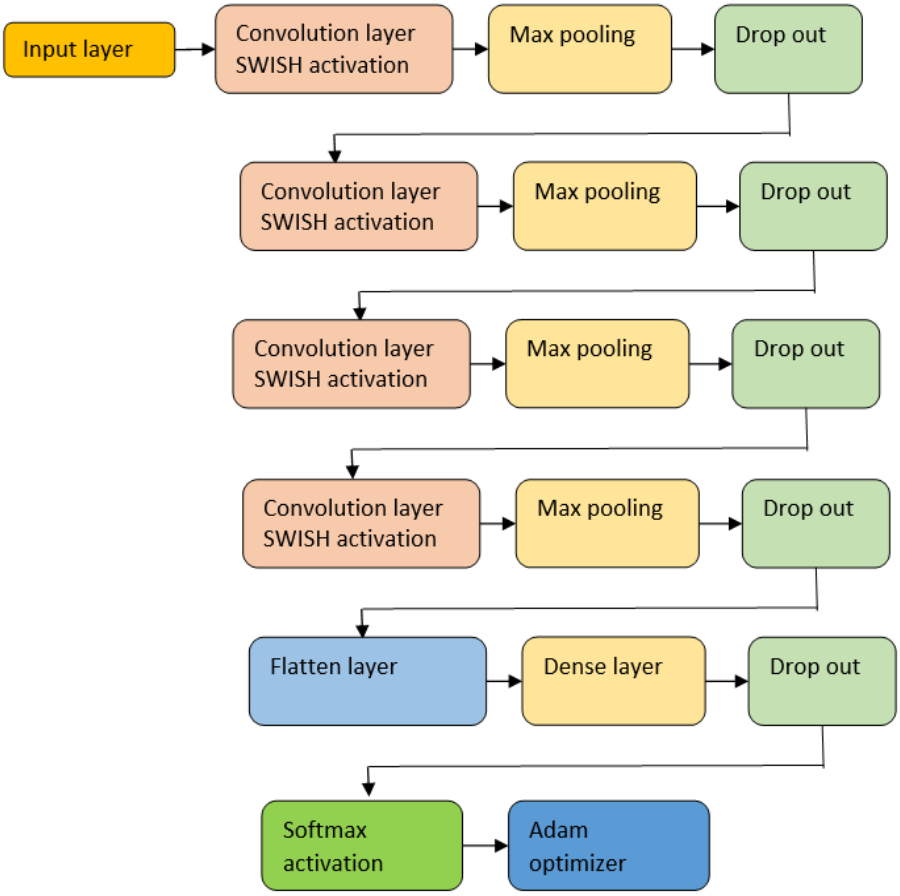

Figure 4. Proposed CNN model with self-activated activation function (SWISH) activation function.

4. EXPERIMENTAL RESULTS

We present the completed classification model here. Like the architecture, the loss function plays a significant role in deep learning. Mild dice loss is frequently used as a loss detection function in segmentation models. When given skewed data, it fares very well. Consequently, it is most useful for a specific kind of cancer research: Segmenting brain tumors.

$$Dice(p,q) = 1 - \frac{2\sum_{i,j} X_{ij} Y_{ij} + \epsilon}{\left(\sum_{i,j} X_{ij}^2\right) + \left(\sum_{i,j} Y_{ij}^2\right) + \epsilon} \quad (9)$$

If p is the prediction and q is the actual data, then the forecast is accurate. We use the small number to avoid a division by zero.

Loss is determined by subtracting 1, so a greater overlap results in a smaller loss, and a smaller overlap results in a greater loss. DSC is a metric used to compare the accuracy of the proposed fully automated process to that of manually defined areas of brain tumours. The "dice score" (DSC) is the fraction of incorrect predictions made out of the total number of predictions made.

$$DSC = \frac{2TP}{FP+TP+FN} \quad (10)$$

$$Dice\ Loss = \frac{2|p_1 \cap q_1|}{|p_1|+|q_1|} \quad (11)$$

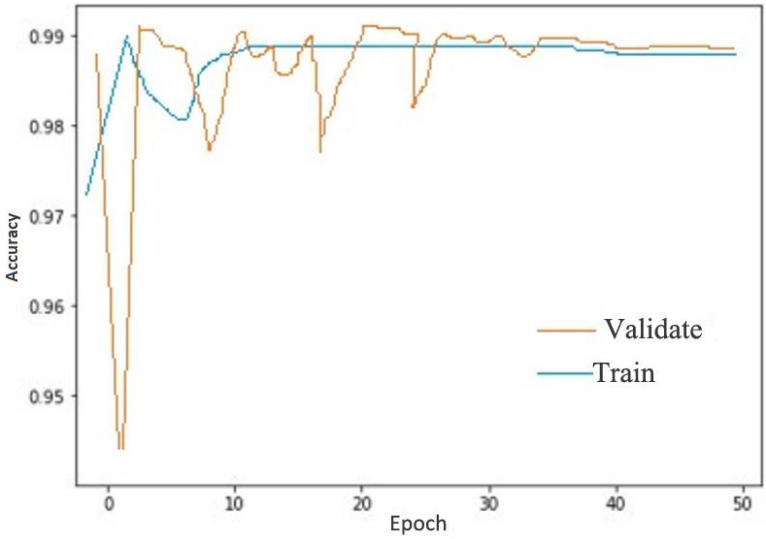

Figure 5. Accuracy for 50 epochs.

Figure 5 shows the accuracy for 50 epochs. Dice coefficients are plotted in Figure 6. The loss function plot is displayed in Figure 7 for the training datasets and validation datasets. The different measures of effectiveness are listed below. The results show that a precision of roughly 99.06% was attained. The results of eight different segmentations are displayed in Figure 8.

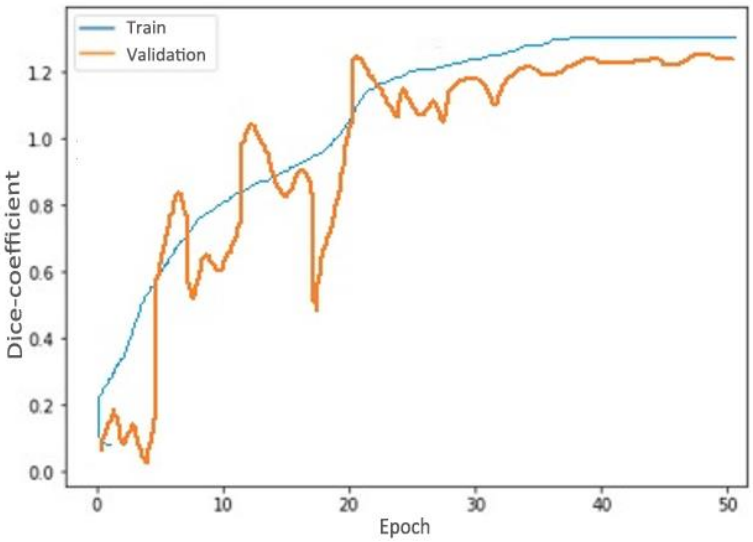

Figure 6. Dice coefficient for 50 epochs.

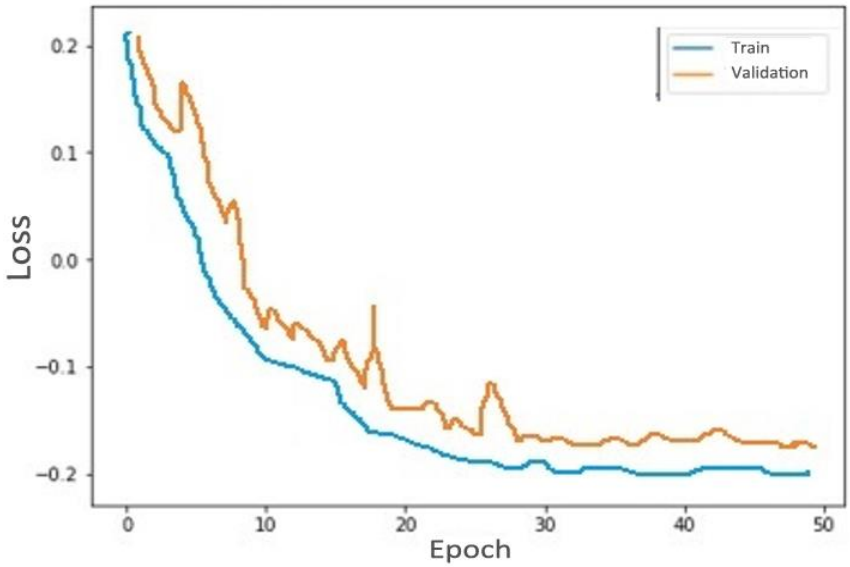

Figure 7. Loss calculation for 50 epochs.

The full data set is shown in Table 1, and dice co-efficient, Loss precision, sensitivity, accuracy, and specificity are all above average (0.17%, 99.06%, 1.28, 088, 0.97, and 0.99) for the model as implemented.

Table 1. Performance measures.

Performance measures	Values
Precision	0.90
Sensitivity	0.98
Specificity	0.99
Dice coefficient	1.24
Accuracy	99.52%
Loss	0.14

The following measures show the classification model's findings.

To what extent is a model classified correctly? Is there one way to judge its effectiveness? To quickly and easily calculate precision using the uncertainty matrix, we can apply the following theorem:

$$Accuracy = \frac{Number\ of\ correct\ predictions}{Total\ number\ of\ predictions} \quad (12)$$

By utilising the labelled and measurable model outputs, loss functions are used to improve the weight vector. The methods of "Gradient Downward" and "Middle-Square-Error" are employed in this paper because of their widespread use and reliability. According to the literature on mathematical optimization and decision theory, an error function or target value can convert a scenario, including one or even more factors, to an actual figure that intuitively represents some cost connected with that scenario. This mapping can take place in either direction.

Precision is defined as the ratio of the number of correct diagnoses to the sum of the numbers of diagnoses that were incorrect.

$$Precision = \frac{TP}{TP+FP} \quad (13)$$

Recall: Sensitivity is the term for remembering something. It is expressed as a fraction of the total found relative instances.

$$Recall = \frac{TP}{TP+FN} \quad (14)$$

F1 Score: In the following equation, it is determined by computing the mean of the weights assigned to the parameters:

$$F1\ score = 2 * \frac{precision * recall}{precision + recall} \quad (15)$$

When dealing with an imbalanced dataset, the F1 score is recommended over precision as it accounts for both false positives and false negatives. This is because the F1 score considers both types of errors. By utilising a weighting parameter, F-measures are used in order to bring the percentage of false - negative into a more even distribution.

$$F = Precision * Recall\ \frac{(1+\beta)^2}{(X+Y)\beta^2} \quad (16)$$

Figure 8 shows the precision versus error function plot for the segmentation phase. As the figure shows, the decline is greatly reduced along with the precision, which peaks at 94.42% with a loss of 0.1691. By reducing the validation loss to 0.5434, the validation accuracy was improved from 87.21% to 87.21%. In Figure 8, we see a plot of the classification model's loss and accuracy across training and validation phases.

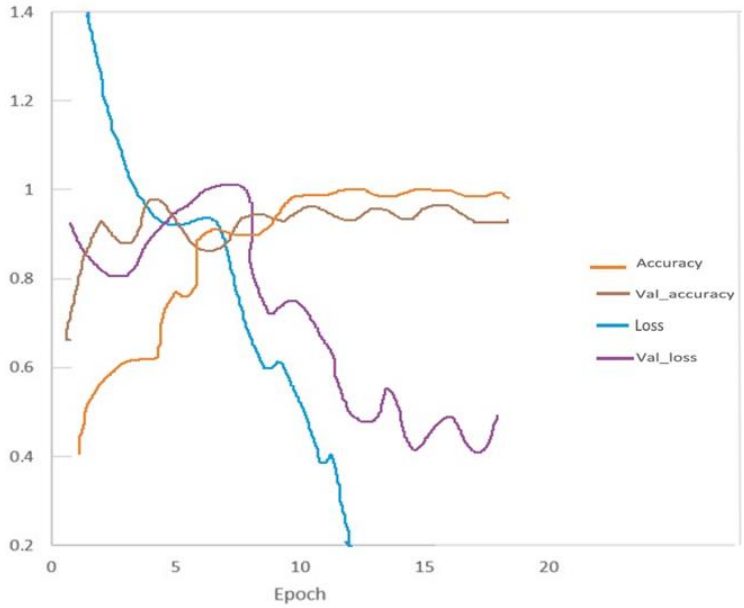

Figure 8. Graph for accuracy and loss.

Following the classification process, the findings of these performance measure assessments are presented in Table 2 for each of the four groups. In the evaluation, there are several categories, such as glioma, that perform badly because of poor precious and remember ratings. This might happen if there aren't enough instances that adequately portray a particular group. A comprehensive model evaluation requires averaging the outcomes. Results from all four classes indicate that the system is operating as intended, with a mean performance of 0.25 in precision, 0.2775 in recall, and 0.23 in F1 score.

Table 2. Metrics for evaluating the effectiveness of the proposed classification scheme.

Metrics	Precision	Recall	F1-score
Glioma	0.26	0.06	0.09
Meningioma	0.26	0.36	0.30
No tumour	0.32	0.48	0.38
Pituitary	0.28	0.21	0.23
Average	0.28	0.2775	0.25

The comparisons of test accuracy and test loss for the specific methods are summarized in Table 3. The proposed classification model has been shown to be more effective than state-of-the-art methods, with better performance and lower loss function values. It has been demonstrated that CNNs and other forms of neural networks have enormous

potential for detecting brain tumors. With the help of a user-friendly website or service, patients can now upload their scans and get an estimate of the tumor's severity. As a result, not only will disease outcomes be better, but so will the availability of these services around the world. These applications may find future use in telemedicine, where patients' scan histories will be stored digitally and made available to their doctors via a website or mobile app, allowing for automated monitoring of tumor growth. As a result, AI will be more useful to more people around the world.

Table 3. Measures of classification performance are compared.

Model	Test accuracy (%)	Test loss
Tensor flow [9]	71	4.5
DNN [3]	67	4.3
Proposed CNN model	99	0.68

5. CONCLUSIONS AND FUTURE ENHANCEMENT

In this research, deep neural networks were used for both brain tumour segmentation and detection. In the current investigation, the neural network is trained using the MRI image dataset, and then segmentation losses are detected using soft dice loss. The model is then trained to correct these losses and return a segmented version of the input image. The initial step in the segmentation process involves slicing the 3D MRI model into smaller 3D sub-models. The CNN models draw on three distinct data sets. To solve the generalisation issue, data is collected from a wide variety of patients all over the world. Second, the CNN algorithm is used specifically for the three most frequent kinds of tumors in the brain—glioma, meningioma, and pituitary—in order to enable rapid classification without the requirement for area-based pre-processing techniques. gliomas are the most common type of brain tumour. The fact that the acquired results are superior to those of other models found in the existing body of research is evidence of the utility of the work that has been proposed.

Despite the exorbitant computing costs, three-dimensional neural networks with deep learning (DNNs) have a significant number of possibilities in a broad range of health applications. These medical image volumes can be significantly shrunk by employing interpolation methods. Accurate tumour localization and early detection can be of great assistance to clinical experts. There may be less room for error and less variation in results as a result of human judgments if this is implemented.

Funding: This study received no specific financial support.
Institutional Review Board Statement: Not applicable.
Transparency: The authors state that the manuscript is honest, truthful, and transparent, that no key aspects of the investigation have been omitted, and that any differences from the study as planned have been clarified. This study followed all writing ethics.
Competing Interests: The authors declare that they have no competing interests.
Authors' Contributions: All authors contributed equally to the conception and design of the study. All authors have read and agreed to the published version of the manuscript. All authors have read and agreed to the published version of the manuscript.

REFERENCES

[1] L. M. De Angelis, "Brain tumors," *The New England Journal of Medicine*, vol. 344, pp. 114-123, 2001.

[2] S. Bakas *et al.*, "Advancing the cancer genome atlas glioma MRI collections with expert segmentation labels and radiomic features," *Scientific Data*, vol. 4, no. 1, pp. 1-13, 2017. https://doi.org/10.1038/sdata.2017.117

[3] R. A. Zeineldin, M. E. Karar, J. Coburger, C. R. Wirtz, and O. Burgert, "DeepSeg: Deep neural network framework for automatic brain tumor segmentation using magnetic resonance FLAIR images," *International Journal of Computer Assisted Radiology and Surgery*, vol. 15, pp. 909-920, 2020. https://doi.org/10.1007/s11548-020-02186-z

[4] S. N. Sangeethaa, "Presumptive discerning of the severity level of glaucoma through clinical fundus images using hybrid PolyNet," *Biomedical Signal Processing and Control*, vol. 81, p. 104347, 2023. https://doi.org/10.1016/j.bspc.2022.104347

[5] C. Zhou, C. Ding, X. Wang, Z. Lu, and D. Tao, "One-pass multi-task networks with cross-task guided attention for brain tumor segmentation," *IEEE Transactions on Image Processing*, vol. 29, pp. 4516-4529, 2020. https://doi.org/10.1109/tip.2020.2973510

[6] F. Milletari, N. Navab, and S. Ahmadi, "V-Net: fully convolutional neural networks for volumetric medical image segmentation," presented at the In: 2016 Fourth International Conference on 3D Vision (3DV), IEEE, 2016.

[7] Z. Akkus, A. Galimzianova, A. Hoogi, D. L. Rubin, and B. J. Erickson, "Deep learning for brain MRI segmentation: State of the art and future directions," *Journal of Digital Imaging*, vol. 30, no. 4, pp. 449-459, 2017. https://doi.org/10.1007/s10278-017-9983-4

[8] A. Zadeh Shirazi *et al.*, "The application of deep convolutional neural networks to brain cancer images: A survey," *Journal of Personalized Medicine*, vol. 10, no. 4, p. 224, 2020. https://doi.org/10.3390/jpm10040224

[9] S. Iqbal, M. U. Ghani, T. Saba, and A. Rehman, "Brain tumor segmentation in multi-spectral MRI using convolutional neural networks (CNN)," *Microscopy Research and Technique*, vol. 81, no. 4, pp. 419-427, 2018.

[10] M. B. Naceur, R. Saouli, M. Akil, and R. Kachouri, "Fully automatic brain tumor segmentation using end-to-end incremental deep neural networks in MRI images," *Computer Methods and Programs in Biomedicine*, vol. 166, pp. 39-49, 2018.

[11] B. H. Menze *et al.*, "The multimodal brain tumor image segmentation benchmark (BRATS)," *IEEE Transactions on Medical Imaging*, vol. 34, no. 10, pp. 1993-2024, 2014.

[12] T. Akilan, Q. J. Wu, A. Safaei, J. Huo, and Y. Yang, "A 3D CNN-LSTM-based image-to-image foreground segmentation," *IEEE Transactions on Intelligent Transportation Systems*, vol. 21, no. 3, pp. 959-971, 2019. https://doi.org/10.1109/tits.2019.2900426

[13] M. A. Balafar, A. R. Ramli, M. I. Saripan, and S. Mashohor, "Review of brain MRI image segmentation methods," *Artificial Intelligence Review*, vol. 33, pp. 261-274, 2010.

[14] Ö. Çiçek, A. Abdulkadir, S. S. Lienkamp, T. Brox, and O. Ronneberger, "3D U-Net: Learning dense volumetric segmentation from sparse annotation," in *Proceedings of the International Conference on Medical Image Computing and Computer-Assisted Intervention, Athens, Greece, 17–21 October 2016; Springer: Cham, Switzerland*, 2016, pp. 424–432.

[15] O. Ronneberger and P. Fischer, "Brox, T. U-net: Convolutional networks for biomedical image segmentation," in *Proceedings of the International Conference on Medical Image Computing and Computer-Assisted Intervention, Munich, Germany, 5–9 October 2015; Springer: Cham, Switzerland*, 2015, pp. 234–241.

[16] M. S. A. Magboo and V. P. C. Magboo, "Detection of brain tumors from MRI images using convolutional neural networks," presented at the 2022 5th International Conference of Computer and Informatics Engineering (IC2IE), Jakarta, Indonesia, 2022.

[17] F. Isensee *et al.*, "Abstract: nnu-net: Self-adapting framework for u-net-based medical image segmentation," *Image Processing for Medicine*, pp. 1-22, 2019. https://doi.org/10.1007/978-3-658-25326-4_7

[18] S. Jégou, M. Drozdzal, D. Vazquez, A. Romero, and Y. Bengio, "The one hundred layers tiramisu: Fully convolutional densenets for semantic segmentation," in *Proceedings of the IEEE Conference on Computer Vision and Pattern Recognition Workshops*, 2017, pp. 11-19.

[19] J. Stawiaski, "A pretrained densenet encoder for brain tumor segmentation," presented at the In Brainlesion: Glioma, Multiple Sclerosis, Stroke and Traumatic Brain Injuries: 4th International Workshop, BrainLes 2018, Held in Conjunction with MICCAI 2018, Granada, Spain, September 16, 2018, Revised Selected Papers, Part II 4, Springer International Publishing., 2019.

[20] R. Ranjbarzadeh, A. Caputo, E. B. Tirkolaee, S. J. Ghoushchi, and M. Bendechache, "Brain tumor segmentation of MRI images: A comprehensive review on the application of artificial intelligence tools," *Computers in Biology and Medicine*, p. 106405, 2022. https://doi.org/10.1016/j.compbiomed.2022.106405

[21] C. Zhou, S. Chen, C. Ding, and D. Tao, "Learning contextual and attentive information for brain tumor segmentation," in *In Brainlesion: Glioma, Multiple Sclerosis, Stroke and Traumatic Brain Injuries: 4th International Workshop, BrainLes 2018,*

Held in Conjunction with MICCAI 2018, Granada, Spain, September 16, 2018, Revised Selected Papers, Part II 4, Springer International Publishing., 2019, pp. 497-507.

[22] Z. W. Zhou and M. R. Siddiquee, "U-Net++: A nested u-net architecture for medical image segmentation," presented at the International Workshop on Deep Learning in Medical Image Analysis Deep Learning in Medical Image Analysis and Multimodal Learning for Clinical Decision Support; Springer: Cham, Switzerland; Berlin/Heidelberg, Germany, 2018.

[23] S. Chen, C. Ding, and M. Liu, "Dual-force convolutional neural networks for accurate brain tumor segmentation," *Pattern Recognition*, vol. 88, pp. 90-100, 2019. https://doi.org/10.1016/j.patcog.2018.11.009

[24] F. Xu, H. Ma, J. Sun, R. Wu, X. Liu, and Y. Kong, "Lstm multimodal unet for brain tumor segmentation," presented at the In: 2019 IEEE 4th International Conference on Image, Vision and Computing (ICIVC), IEEE, 2019.

[25] O. Kouli, A. Hassane, D. Badran, T. Kouli, K. Hossain-Ibrahim, and J. D. Steele, "Automated brain tumor identification using magnetic resonance imaging: A systematic review and meta-analysis," *Neuro-Oncology Advances*, vol. 4, no. 1, p. vdac081, 2022. https://doi.org/10.1093/noajnl/vdac081

[26] J. Wu and X. Tang, "Brain segmentation based on multi-atlas guided 3D fully convolutional network ensembles," *Pattern Recognition*, vol. 115, p. 107904, 2019. https://doi.org/10.1016/j.patcog.2021.107904

[27] Z. Tang, S. Ahmad, P.-T. Yap, and D. Shen, "Multi-atlas segmentation of MR tumor brain images using low-rank based image recovery," *IEEE Transactions on Medical Imaging*, vol. 37, no. 10, pp. 2224-2235, 2018. https://doi.org/10.1109/tmi.2018.2824243

[28] G. Urban, M. Bendszus, F. Hamprecht, and J. Kleesiek, "Multi-modal brain tumor segmentation using deep convolutional neural networks. MICCAI BraTS (brain tumor segmentation) challenge," in *Proceedings, Winning Contribution*, 2014, pp. 31-35.

[29] M. Noori, A. Bahri, and K. Mohammadi, "Attention-guided version of 2d unet for automatic brain tumor segmentation," presented at the In: 2019 9th International Conference on Computer and Knowledge Engineering (ICCKE), IEEE, 2019.

[30] S. M. Kurian and S. Juliet, "An automatic and intelligent brain tumor detection using Lee sigma filtered histogram segmentation model," *Soft Computing*, vol. 27, pp. 13305–13319, 2023. https://doi.org/10.1007/s00500-022-07457-2

[31] Y. Sun, C. Zhou, Y. Fu, and X. Xue, "Parasitic GAN for semi-supervised brain tumor segmentation," in *Proceedings of the 2019 IEEE International Conference on Image Processing (ICIP), Taipei, Taiwan, 22–25 September 2019; IEEE: Piscataway, NJ, USA*, 2019, pp. 1535–1539.

[32] X. Gan, L. Wang, Q. Chen, Y. Ge, and S. Duan, "GAU-Net: U-Net based on global attention mechanism for brain tumor segmentation," In Journal of Physics: Conference Series (Vol. 1861, No. 1, p. 012041). IOP Publishing, 2021.